Thermodynamics of the ATPase Cycle of GlcV, the Nucleotide-Binding Domain of the Glucose ABC Transporter of *Sulfolobus solfataricus*†

Monika G. Pretz,‡ Sonja-Verena Albers,‡ Gea Schuurman-Wolters,§ Robert Tampé,|| Arnold J. M. Driessen,*,‡ and Chris van der Does‡

Department of Molecular Microbiology, University of Groningen, Groningen, The Netherlands, Department of Biochemistry, University of Groningen, Groningen, The Netherlands, and Institute of Biochemistry, Johann Wolfgang Goethe-University, Frankfurt am Main, Germany

Received June 20, 2006; Revised Manuscript Received October 10, 2006

ABSTRACT: ATP-binding cassette transporters drive the transport of substrates across the membrane by the hydrolysis of ATP. They typically have a conserved domain structure with two membrane-spanning domains that form the transport channel and two cytosolic nucleotide-binding domains (NBDs) that energize the transport reaction. Binding of ATP to the NBD monomer results in formation of a NBD dimer. Hydrolysis of the ATP drives the dissociation of the dimer. The thermodynamics of distinct steps in the ATPase cycle of GlcV, the NBD of the glucose ABC transporter of the extreme thermoacidophile *Sulfolobus solfataricus*, were studied by isothermal titration calorimetry using the wild-type protein and two mutants, which are arrested at different steps in the ATP hydrolytic cycle. The G144A mutant is unable to dimerize, while the E166A mutant is defective in dimer dissociation. The ATP, ADP, and AMP-PNP binding affinities, stoichiometries, and enthalpies of binding were determined at different temperatures. From these data, the thermodynamic parameters of nucleotide binding, NBD dimerization, and ATP hydrolysis were calculated. The data demonstrate that the ATP hydrolysis cycle of isolated NBDs consists of consecutive steps where only the final step of ADP release is energetically unfavorable.

ATP-binding cassette (ABC)[1] transporters represent one of the largest superfamilies of primary transporters (*1*). They are found in all phyla of life and are responsible for many physiological processes ranging from solute uptake to multidrug resistance. ABC transporters have a conserved domain structure and consist of two membrane-spanning domains (MSDs) that form the transport pathway and two cytosolic nucleotide-binding domains (NBDs) that energize the transport via the hydrolysis of ATP. The amino acid sequences of the MSDs are dimers, while the NBDs are highly conserved with amino acid sequence motifs that are involved in the binding of nucleotides.

Several structures of full-length ABC transporters and of many isolated NBDs have been determined. The structures of the NBDs are highly conserved (for reviews, see refs *2*−*5*). The NBD monomer forms an L-shaped molecule with two domains. Lobe I includes the ATP-binding core domain with the Walker A and B motifs. This domain contains central β-sheets which are flanked by α-helices. Residues of the Walker A motif interact with the phosphates of ATP and ADP, while an aspartate of the Walker B motif coordinates the magnesium ion. The glutamate immediately following this aspartate most likely coordinates the water molecule that attacks the γ-phosphate and thus may function as a catalytic base. Recently, it was suggested that this glutamate functions in a catalytic dyad together with the conserved histidine in the H-loop (*6*). The characteristic ABC signature motif is located in the second domain, which is called lobe II, and is far from the nucleotide that is bound to lobe I. In the presence of ATP, two monomers form a dimer in which the monomers are oriented in a head-to-tail configuration with two ATP molecules bound at the subunit interface. These are sandwiched between the Walker A and B motifs from one monomer and the C-loop of the other that complements the nucleotide-binding site (*6*−*10*). Analysis of the structures of various NBDs in the ADP-bound and free states reveals only minor structural differences, while when ATP binds, a large rigid body movement of lobe I toward lobe II occurs. This rigid body movement aligns the monomers in such a manner that the dimer can be formed as a kind of "induced fit". ATP, and in particular the γ-phosphate, occupies a significant part of the dimer interface, and many residues of the NBDs contact the bound nucleotide rather than residues of the opposite dimer. In this way, ATP stabilizes the dimeric state (*8*), while hydrolysis of ATP results in the loss of many of the dimer-stabilizing

† This work was supported by a MEMBMACS training network and funded by EU TMR Contract HPRN-CT-2000-00075. C.v.d.D. and S.-V.A. were supported by TALENT and VENI fellowships of the Netherlands Organization for scientific research (NWO).

* To whom correspondence should be addressed. E-mail: a.j.m.driessen@rug.nl. Phone: 0031-50-3632170. Fax: 0031-50-3632154.

‡ Department of Molecular Microbiology, University of Groningen.

§ Department of Biochemistry, University of Groningen.

|| Johann Wolfgang Goethe-University.

[1] Abbreviations: ABC, ATP-binding cassette; MSD, membrane-spanning domain; NBD, nucleotide-binding domain; TMH, transmembrane helix; ITC, isothermal titration calorimetry; ΔC_p, heat capacity; ΔG, Gibbs free energy; $\Delta G^{\ddagger}$, free activation enthalpy; ΔH, enthalpy; $\Delta H^{\ddagger}$, activation enthalpy; ΔS, entropy; $-T\Delta S^{\ddagger}$, free activation entropy; DLS, dynamic light scattering; AMP-PNP, adenosine (β,γ-imido)-triphosphate.

10.1021/bi061230e CCC: $33.50
Published on Web 11/22/2006

interactions. Next to the monomeric and dimeric states, a slightly opened nucleotide-free state was observed for *Escherichia coli* MalK (*10*). In this state, the dimer is maintained through contacts between the C-terminal regulatory domains, which is an extra domain found in several NBDs like in *Sulfolobus solfataricus* GlcV (see below). Addition of Mg^{2+} to the ATP-bound dimer resulted in an opened posthydrolytic ADP-Mg^{2+}-bound state which showed that ADP-Mg^{2+} is unable to stabilize the closed dimer (*11*). Thus, the closed dimer was observed only in the presence of ATP and never in the presence of ADP or AMP-PNP.

How ATP hydrolysis occurs in detail is currently a matter of debate. Several different models have been proposed, e.g., the "alternating catalytic site" and the "processive clamp" model. The alternating site model (*12*) is based on transition state mutants of *E. coli* $MalFGK_2$ (*13*) and P-gp (*14*) transporters where one single nucleotide binds to the NBDs. This model suggests that ATP hydrolysis occurs in the first catalytic site, followed by opening of this domain while the second catalytic site remains closed. Additional ATP binding then induces closure of the first site and leads to ATP hydrolysis in the second site. Thus, hydrolysis would take place without complete dissociation of the dimer. The processive clamp or "ATP switch" models (*3*, *15*, *16*) are based on biochemical and structural data obtained with isolated NBDs that showed that two ATP molecules are bound in the dimeric state and on kinetic data that showed that association and dissociation of the dimer are important steps in the ATP hydrolysis cycle (*17*). These data suggest that ATP molecules bind to the two monomers, resulting in the formation of the dimer, whereupon the hydrolysis of both ATP molecules subsequently results in dissociation of the dimer (*5*).

The intimate features of the ATP hydrolytic cycle and how this process is coupled to the transport mechanism remain to be elucidated. A thermodynamic analysis of nucleotide binding and hydrolysis can provide detailed information about the energetics of nucleotide binding and the conformational changes that are associated with nucleotide binding and hydrolysis and with dimerization of the NBDs. Recently, the thermodynamics of the transition state of the ATP hydrolysis cycle of Pgp was studied by determining the ATP hydrolysis rate as a function of the temperature and application of the Arrhenius and Eyring equations (*18*). This study demonstrated two different transition states in the presence and absence of substrates. The approach that was used, however, allowed the determination of the thermodynamics of only the rate-limiting step. Here we set out to study the thermodynamics of different steps in the ATP hydrolysis cycle. Such studies are typically conducted by isothermal titration calorimetry (ITC). ITC experiments are facilitated by the use of thermostable proteins that allow the determination of the change in heat capacity (ΔC_p) of a ligand binding event over a wide range of temperatures. To analyze the thermodynamics of the ATP hydrolytic cycle of an isolated NBD, we have employed the NBD of the glucose ABC transporter of the extreme thermoacidophile *S. solfataricus* (*19*). This transporter consists of five proteins: the heterodimeric MSDs (GlcT and GlcU), two copies of the NBD (GlcV) forming a homodimer, and the glucose binding protein (GlcS). GlcV has been crystallized in a monomeric form in the nucleotide-free, ADP-Mg^{2+}-bound, and AMP-PNP-Mg^{2+}-bound states (*20*). The structure of GlcV exhibits a fold similar to those of other NBDs, but it contains an additional C-terminal domain that is connected to the NBD via a linker region. The function of this C-terminal domain is unknown, but its sequence is 28% identical to that of the regulatory domain of MalK that is responsible for the binding of MalT, the positive regulator of the *mal* operon (*21*). In both structures, the C-terminal domain has a similar β-barrel structure. The MalK structure contains an additional connecting α-helix (*22*), while in GlcV, it contains only a loop region between β13 and β14 (*20*). The isolated GlcV and mutants have been characterized biochemically (*23*). The ATPase activity of wild-type GlcV is too high to allow the detection of a dimer in solution. Mutation of the conserved glutamate downstream of the Walker B motif of GlcV (E166Q) resulted in a strongly reduced ATPase activity, and this allowed demonstration of ATP-dependent dimerization of GlcV (*23*). Substitution of the glutamate for alanine resulted in a GlcV mutant that is inactive for ATP hydrolysis and that required both ATP and Mg^{2+} for dimer formation. Finally, mutation of the second glycine (G144A) in the C-loop motif also resulted in an inactive protein, but this mutant also failed to dimerize. This indicated an essential role of this residue in the stabilization of the productive dimeric state.

To study the thermodynamics of binding of nucleotides to GlcV, we have employed the wild-type (wt) protein which is highly active in ATP hydrolysis and two of the mutants that still bind nucleotide but that are inactive in ATP hydrolysis and arrested at different intermediate stages in the catalytic cycle. The use of these three proteins allowed the determination of kinetic and thermodynamic parameters of nucleotide binding at the different steps of the ATP hydrolytic cycle.

MATERIALS AND METHODS

Expression and Purification. S. solfataricus wt GlcV and the E166A and G144A mutant were expressed in *E. coli* and purified as described previously (*20*, *23*, *24*).

Size-Exclusion Chromatography. Size-exclusion chromatography was used to analyze the oligomeric state of wt and mutant GlcV proteins. GlcV (30 μM) was incubated for 5 min at 20 °C in 20 mM MES (pH 6.5), 100 mM NaCl, and 5 mM $MgCl_2$ or 2 mM EDTA in the presence of different concentrations of ATP. Samples were applied to a Superdex 200 size-exclusion column (PC 3.2/30; bed volume of 2.4 mL) mounted on a SMART system (Amersham Biosciences) equilibrated with the same buffer containing an equal concentration of ATP at 20 °C and at a flow rate of 75 μL/min. The molecular mass was determined using molecular mass standards: ribonuclease A (14 kDa), chymotrypsinogen A (25 kDa), ovalbumin (44 kDa), albumin (67 kDa), and γ-globulin (158 kDa).

ATP Binding and Hydrolysis Assay. ATP binding was assessed by means of 8-azido-ATP photolabeling. GlcV (10 nM) was added to a premixed solution of 15 nM 8-azido-[γ-^{32}P]ATP in the presence of increasing concentrations (from 0 to 2 μM) of ATP in binding buffer [20 mM MES (pH 6.5), 100 mM NaCl, and 5 mM $MgCl_2$]. After being incubated for 5 min on ice, samples were irradiated by UV (254 nm) for 2 min, directly resuspended in SDS loading

buffer, and separated by 12% SDS−PAGE. Gels were dried and quantified by phosphorimaging. ATP hydrolysis was assessed using radiolabeled [γ-^{32}P]ATP (10 mCi, 3000 Ci/mmol). wt and mutant GlcV (30 μM) were incubated at different temperatures with 3 μM or 5 mM [γ-^{32}P]ATP in 50 μL of 50 mM MES (pH 6.5) and 100 mM NaCl, in the presence of 5 mM $MgCl_2$ or 2 mM EDTA. The reaction was stopped after 0−10 min by the addition of 950 μL of 10% (w/v) charcoal in 10 mM EDTA. Solutions were mixed and incubated for 3 h to allow ATP to bind to the charcoal. The mixture was then centrifuged for 15 min at 14000*g*, and the radioactivity in the supernatant was measured by liquid scintillation counting. To assess nonspecific ATP binding, control experiments were performed under identical conditions in the absence of GlcV. Blank values were subtracted from the total counts, and the total extent of hydrolysis was calculated.

Dynamic Light Scattering. Dynamic light scattering experiments were performed with a Dynapro 801 device. Before use, GlcV and nucleotide solutions were filtered and concentrations in the filtrate were determined spectrophotometrically. Before injection, 30 μM E166A or G144A GlcV protein was incubated for 5, 15, and 30 min in 20 mM MES (pH 6.5), 100 mM NaCl, and 5 mM $MgCl_2$ or 2 mM EDTA at 20 °C in the absence and presence of different ATP concentrations. After the samples had been injected into the measuring chamber, the diffusion coefficient and the apparent molecular mass were determined from the light scattering using Dynamics version 5.26.37 (Protein Solution Inc.). Translational diffusion coefficients of monomeric and dimeric GlcV were predicted using HYDROPRO version 5.a (*25*).

Isothermal Titration Calorimetry (ITC). Binding of nucleotides to GlcV was analyzed using a Microcal MCS titration calorimeter (Microcal). Stock solutions (100 mM) of the nucleotides (ATP, ADP, or AMP-PNP) were prepared, adjusted to pH 6.5 with NaOH, and diluted in dialysis buffer. Purified wt GlcV and the G144A and E166A mutants were dialyzed against 20 mM MES (pH 6.5), 100 mM NaCl, and 5 mM $MgCl_2$, or when indicated against 20 mM MES (pH 6.5), 100 mM NaCl, and 2 mM EDTA. Before use, all solutions were degassed by being gently stirred under vacuum. ITC experiments were performed by injecting nucleotide into the sample cell containing the purified GlcV proteins. The instrument and the equations used to fit the calorimetric data have been described in detail previously (*26*). In a typical experiment, the 2.1 mL sample cell was filled with a 30 μM protein solution. Typically, 20 injections (10.6 s duration) of 5 μL of a 600 μM nucleotide solution were made at 180 s intervals from a 100 μL syringe rotating at 400 rpm. At 20 and 30 °C, injection intervals were increased to 600 s for the G144A and E166A mutants. Control experiments to determine the dilution effects of the nucleotides were performed under identical conditions with the sample cell filled with buffer only.

Miscellaneous Methods. Protein and nucleotide concentrations were determined spectrophotometrically at 280 and 260 nm using extinction coefficients of 20 000 and 14 900 M^{-1} cm^{-1}, respectively. The spectroscopic analysis of protein was confirmed by determination of the total amino acid content (Eurosequence).

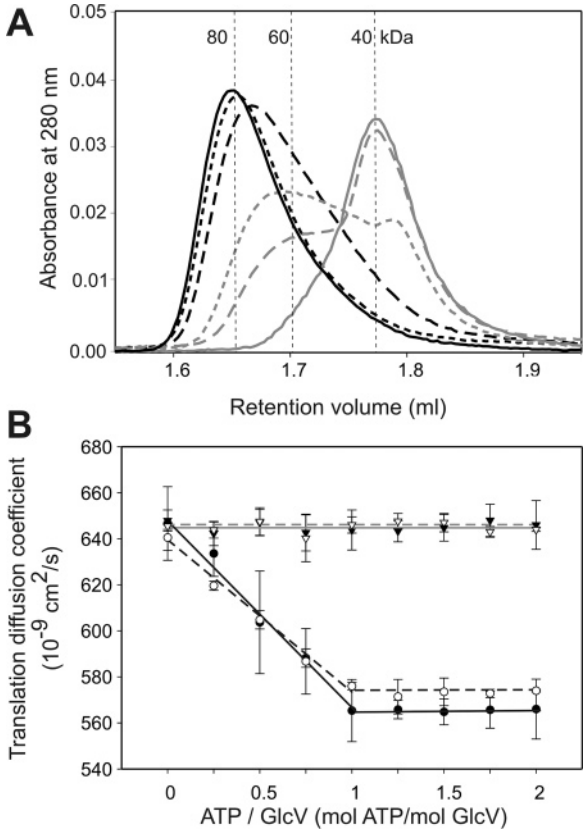

FIGURE 1: E166A GlcV dimerizes in the absence of glycerol. (A) The GlcV E166A mutant (30 μM) was preincubated in the presence of different concentrations of ATP (gray line, no ATP; long dashed gray line, 0.94 μM ATP; short dashed gray line, 1.87 μM ATP; long dashed black line, 3.75 μM ATP; short dashed black line, 7.5 μM ATP; black line, 30 μM ATP) in 20 mM MES (pH 6.5), 100 mM NaCl, and 5 mM $MgCl_2$ and applied to a gel filtration column equilibrated with the same ATP and buffer concentrations. (B) Dynamic light scattering experiments of the E166A (circles and black lines) and G144A (triangles and gray lines) mutants in the presence of 5 mM Mg^{2+} (filled symbols and solid lines) or 2 mM EDTA (empty symbols and dashed lines).

RESULTS

Stabilization of the GlcV Dimer. To analyze the thermodynamics of the ATPase cycle of GlcV, the NBD of the glucose transporter of *S. solfataricus*, we used mutants that are arrested at different stages of the catalytic cycle. The G144A and E166A mutants, which carry mutations in the C-loop and in the residue directly after the aspartate of the Walker B binding motif, have strongly reduced ATPase activity (*23*). In the presence of ATP, the E166A mutant of GlcV exhibited ATP-dependent dimerization as shown by size-exclusion chromatography, whereas wt GlcV and the G144A mutant eluted as monomers (*23*). This dimerization, however, is observed only when ATP is present in the elution buffer, suggesting that the E166A dimer is in a dynamic equilibrium with the monomer and readily dissociates on the size-exclusion column. Therefore, we searched for conditions that yielded a more stable E166A dimer. Remarkably, in the absence of glycerol in the elution buffer, the E166A mutant eluted as a dimer even under conditions where ATP was present in substoichiometric amounts (Figure 1A). In the absence of ATP, or at very low ATP concentrations, GlcV eluted as a monomer. Analysis of the absorption at 260 nm showed that ATP from the running buffer remained bound

to GlcV (data not shown). Since the NBD elutes faster from the column than the nucleotide, it will constantly encounter and bind fresh nucleotides. Apparently, the nucleotides remain bound to the NBD. This suggests a high binding affinity for nucleotides and explains why substoichiometric ATP concentrations already sufficed to stabilize the dimeric form. This also explains the small shift in the elution volume of the dimeric species at lower ATP concentrations, since some of the dimer is formed only after injection on the column. Remarkably, in the absence of glycerol and Mg^{2+} but in the presence of EDTA, similar results were obtained (data not shown). This shows that even in the absence of Mg^{2+}, the GlcV E166A ATP-bound dimer is stable in a buffer without glycerol.

To determine the extent of dimerization and the ATP dependence under steady state conditions, the translational diffusion coefficient of the E166A mutant was determined by dynamic light scattering (DLS). DLS experiments in the absence of ATP resulted in a diffusion coefficient of 646×10^{-9} cm^2/s (Figure 1B). The observed translational diffusion coefficient decreased with ATP concentration but remained stable (565×10^{-9} cm^2/s) when ATP was present in greater than stoichiometric amounts relative to the GlcV monomer (Figure 1B). A further increase in the ATP concentration was without effect, suggesting that the NBD dimer contains two nucleotides. As observed in the gel filtration experiments, the E166A mutant stably dimerizes in an ATP-dependent manner both in the presence and in the absence of Mg^{2+} (Figure 1B). On the other hand, the G144A mutant showed a translational diffusion coefficient of 644×10^{-9} cm^2/s and remained unaffected by the ATP concentration, confirming the previous findings that this mutant remains monomeric in the presence of ATP (*23*). The maximal ($\sim 645 \times 10^{-9}$ cm^2/s) and minimal ($\sim 570 \times 10^{-9}$ cm^2/s) translational diffusion coefficients corresponded to globular proteins of 54 and 73 kDa, respectively. Monomeric GlcV is an elongated protein with a molecular mass of 39.1 kDa, while the proposed dimeric GlcV has a more spherical shape. When HYDROPRO (*25*) was used to predict translational diffusion coefficients based on the crystal structures of GlcV, values of 683×10^{-9} and 578×10^{-9} cm^2/s were obtained for the monomeric and dimeric protein, respectively. These numbers fit well with the observed data showing that the E166A mutant stably dimerizes both in the presence and in the absence of EDTA in a buffer that is devoid of glycerol. Neither for wt GlcV nor for the mutants was dimerization observed in the presence of ADP or AMP-PNP (data not shown).

ATPase Activities of Wild-Type and Mutant GlcV Proteins. wt GlcV has an optimal ATPase activity at pH 6.5 and 80 °C (M. G. Pretz et al., manuscript in preparation), while no ATPase activity could be detected for the G144A and E166A mutants using the malachite green ATPase assay (*24*). Using a sensitive method based on radiolabeled [γ-^{32}P]ATP, the E166A mutant exhibited ~1% of the activity of wt GlcV in the presence of 5 mM ATP, while no ATPase activity was detectable with the G144A mutant (Figure 2A). The thermodynamics of the transition state of a reaction can be determined by measuring the reaction rate as a function of temperature and application of the Eyring equation. The determination of the activation entropy ($-T\Delta S^{\ddagger}$), which is derived from the *y*-intercept of the Eyring plot, is for

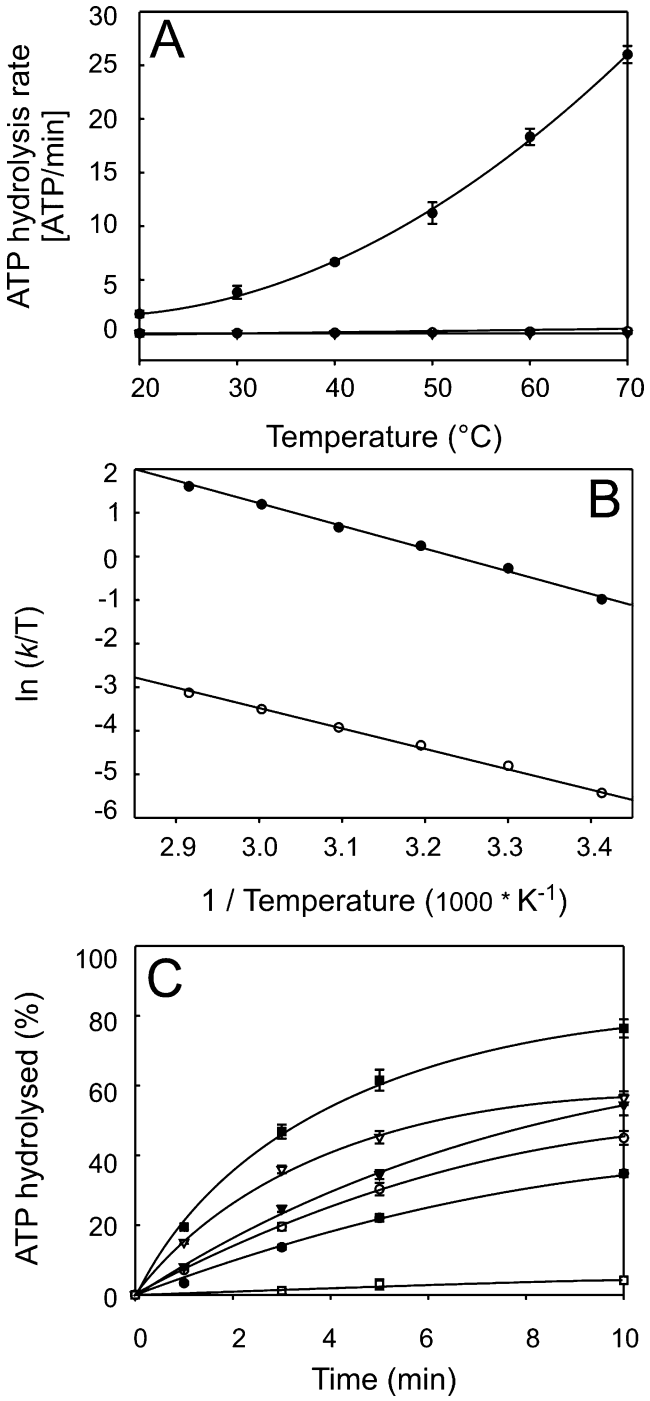

FIGURE 2: ATP hydrolysis of wt GlcV and the G144A and E166A mutants. (A) ATP hydrolysis rate at 5 mM Mg^{2+}-ATP and 30 μM GlcV as a function of temperature [wt (●), E166A (○), and G144A (▼)]. (B) Eyring plot of the ATP hydrolysis rates of wt GlcV (●) and the E166A mutant (○). (C) Percentage of ATP hydrolyzed when 3 μM Mg^{2+}-ATP is incubated in the presence of 30 μM E166A-GlcV at 20 (●), 30 (○), 40 (▼), 50 (▽), and 60 °C (■) as a function of time. The empty squares depict the background of ATP hydrolysis of E166A GlcV in the presence of EDTA at 60 °C.

mesophilic enzymes rather inaccurate since the rates can often be determined only over a small temperature range of 15−20 °C. We were, however, able to determine the ATP hydrolysis rate of GlcV over a range of 60 °C. Analysis of the temperature dependence of the ATPase activity (Figure 2B) yielded rather similar activation enthalpies ($\Delta H^{\ddagger}$) for ATP hydrolysis of 10.3 and 9.2 kcal/mol for the wt and E166A mutant, respectively. Larger differences were, how-

ever, observed between the wt and E166A mutant for the free activation enthalpy ($\Delta G^{\ddagger}$), 14.9 and 18.0 kcal/mol, respectively, and the free activation entropy ($-T\Delta S^{\ddagger}$), 4.6 and 8.8 kcal/mol, respectively. Thus, while the enthalpy change to reach the transition state is approximately similar for the wt and the E166A mutant, the lower reaction rate of the E166A mutant is a result of the more positive $-T\Delta S^{\ddagger}$ of its transition state. This suggests that the transition state of the E166A mutant has a more ordered or more rigid structure than the transition state of the wt protein.

Next to the thermodynamics of the transition state, we also set out to determine the thermodynamics of different steps in the ATP hydrolysis cycle. Since even a small remaining ATPase activity can influence the analysis of the ITC measurements, the ATPase activities of wt and mutant GlcV proteins were determined under conditions that are used in the ITC experiments, i.e., 30 μM GlcV and 3 μM ATP per injection. Under those conditions, the concentration of ATP during a single injection is 10-fold lower than the protein concentration and all ATP was hydrolyzed within the first minute in the presence of wt GlcV. Even after 20 consecutive injections, ATP was hydrolyzed within 1 min by wt GlcV (data not shown). Therefore, accumulation of ADP does not noticeably inhibit the ATPase activity of wt GlcV under the conditions of the ITC experiments. The E166A mutant exhibited still significant ATPase activity under these conditions [50% hydrolyzed after an injection for 3 min at 60 °C (Figure 2C)], while the activity of the G144A mutant was negligible (<3% hydrolyzed after an injection for 3 min at 60 °C) (data not shown). Remarkably, the E166A mutant hydrolyzed only part of the ATP after consecutive injections with ATP. The ITC profile of the E166A mutant in the presence of Mg^{2+} therefore will reflect nucleotide binding, dimerization, and partial hydrolysis. In the absence of Mg^{2+}, the E166A mutant was inactive for ATP hydrolysis (Figure 2C), although the protein still dimerizes under these conditions. Thus, ATP binding experiments with the E166A mutant in the absence of Mg^{2+} will yield an ITC profile that reflects only nucleotide binding and the conformational changes that result in dimerization.

To determine if the G144A mutant still binds ATP, 8-azido-ATP photolabeling experiments were conducted. wt, G144A, and E166A GlcV could be photolabeled with 8-azido[γ-^{32}P]ATP, while the labeling was specifically challenged by an excess of unlabeled ATP (Figure 3A). At 20 °C, the three proteins exhibited binding affinities in the nanomolar range, with the E166A mutant binding with a slightly higher affinity. Due to the high affinity, small amounts of protein and 8-azido-ATP were used in the experiments, and therefore, it was difficult to reduce the error in the experiment and to obtain an accurate estimation of the affinity (data not shown). Although the G144A mutant is unable to hydrolyze ATP or to dimerize, the experiment clearly shows that this mutant still binds ATP with high affinity. Indeed, in the monomeric NBD structures, this residue is not part of the ATP-binding site. Therefore, ATP binding experiments with the G144A mutant both in the absence and in the presence of Mg^{2+} will yield an ITC profile that only reflects nucleotide binding without dimerization. We therefore conclude that the three proteins (wt, G144A, and E166A) reflect different intermediates of the ATP hydrolytic cycle of GlcV.

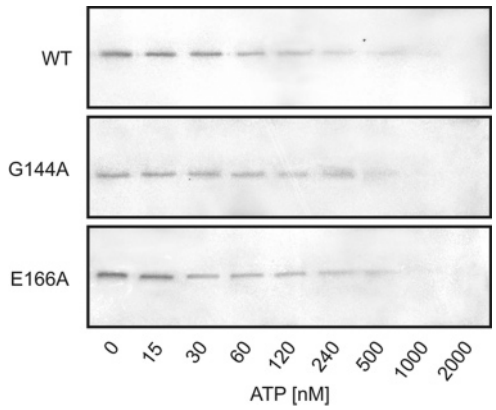

FIGURE 3: 8-Azido-ATP photolabeling of wt and the G144A and E166A mutants. 8-Azido[γ-^{32}P]ATP (15 nM) was bound to the purified NBD (10 nM) and challenged with increasing concentrations (0−2 μM) of nucleoside triphosphates in binding buffer.

Thermodynamics of Binding of a Nucleotide to Wild-Type and Mutant GlcV Proteins. The thermodynamics of binding of a nucleotide to GlcV was investigated by ITC. This method directly measures the heat of the reaction (enthalpy, ΔH), the stoichiometry of substrate binding (n), and the binding affinity of the substrate (K_a). From these values, the Gibbs free energy of association ($\Delta G = -RT \ln K_a$) and the entropy ($T\Delta S = \Delta H - \Delta G$) can be calculated. Furthermore, on the basis of the dependence of the enthalpy on the temperature, changes in the heat capacity ($\Delta C_p = \Delta H/\Delta T$) can be determined. ITC profiles for the different nucleotides were recorded at various temperatures. Above 60 °C, the ITC profiles became noisy while the binding affinity of AMP-PNP and ATP in the absence of Mg^{2+} became too low to be determined accurately. Therefore, the experiments were performed at 20, 30, 40, 50, and 60 °C. First, the thermodynamics of binding of ADP and AMP-PNP to the wt and mutant GlcV proteins in the presence of Mg^{2+} were determined. Figures 4 and 5 show typical ITC titration curves for the binding of ADP at 60 °C (Figure 4A) and of AMP-PNP at 40 °C (Figure 5A). In Figures 4B and 5B, the calculated values for ΔG, ΔH, and $-T\Delta S$ for the binding of ADP and AMP-PNP to wt and mutant GlcV proteins are shown for the temperature range of 20−60 °C. Table 1 summarizes the thermodynamic parameters, nucleotide binding affinities, and stoichiometries that were calculated from the ITC experiments. As expected, ADP and AMP-PNP binding occurs with a stoichiometry of ∼1 (Table 1). Compared to that for ADP, the affinity for AMP-PNP was reduced 100-fold. The K_d values for binding of ADP and AMP-PNP to the various GlcV proteins were essentially indistinguishable, except for the E166A mutant that showed a reduced binding affinity for ADP. The affinities decreased with an increase in temperature and reached lower micromolar values at the optimal growth temperature (80 °C) of *S. solfataricus*, which is within the same range as binding affinities observed for other NBDs of ABC transporters (*15*, *27*−*29*). The ΔG, ΔH, and $-T\Delta S$ values for AMP-PNP binding were much smaller than those observed for ADP. For ADP, the binding reaction was associated with a large negative ΔH and opposed by a positive $-T\Delta S$. The ΔH for ADP binding exhibited distinct temperature dependence, whereas the ΔH for AMP-PNP binding was much smaller and temperature-independent (Figures 4B and 5B). The

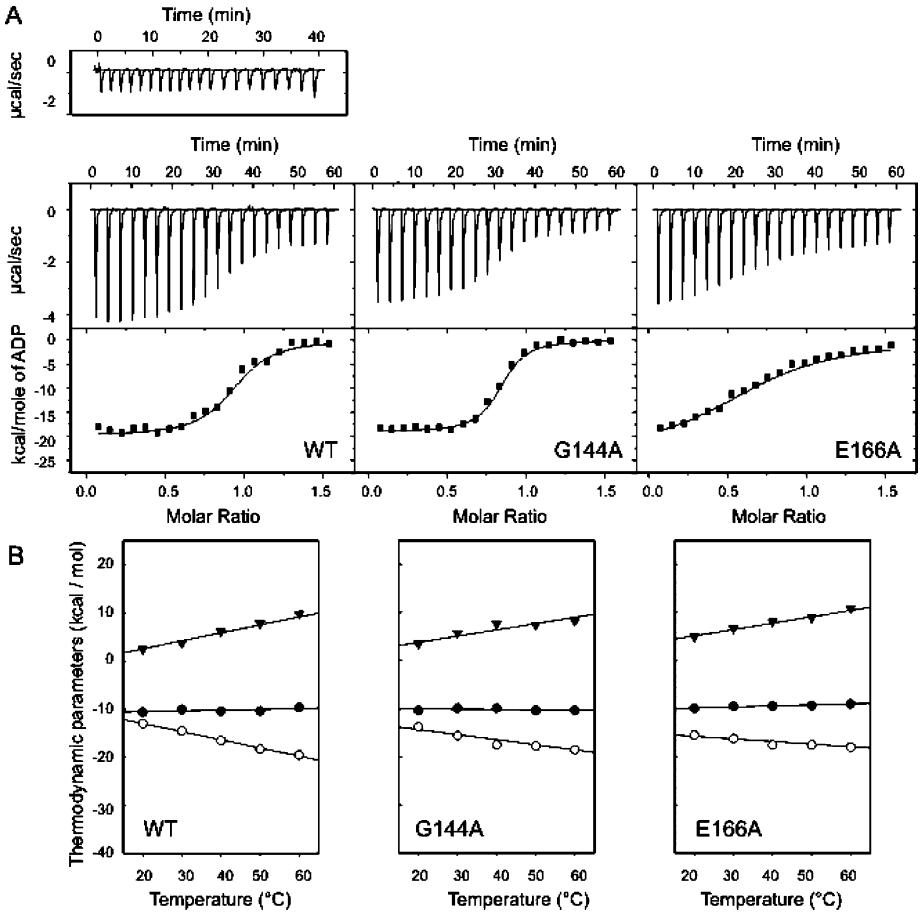

FIGURE 4: Isothermal titration calorimetry of binding of Mg^{2+}-ADP to wt GlcV and the G144A and E166A mutants. (A) The top panel depicts the dilution effect of the titration of Mg^{2+}-ADP at 60 °C. The middle panel depicts the binding isotherm for the titration of wt GlcV and the G144A and E166A mutants with Mg^{2+}-ADP at 60 °C. Twenty injections of 5 μL of a 600 μM nucleotide solution were made at 180 s intervals in a volume of 2.1 mL containing 30 μM protein. The area under each injection signal was integrated, and in the bottom panel, the enthalpy per mole of nucleotide injected is plotted vs the nucleotide:NBD molar ratio. The solid line represents a nonlinear least-squares fit of the reaction heat for the injection. (B) Temperature dependence of the thermodynamic parameters of ADP-Mg^{2+} binding from 20 to 60 °C: (○) ΔH, (●) ΔG, and (▼) $-T\Delta S$.

temperature dependence of ADP binding corresponded to a ΔC_p of -167 cal mol^{-1} K^{-1} for wt GlcV, -94 cal mol^{-1} K^{-1} for G144A, and -115 cal mol^{-1} K^{-1} for E166A. These values are relatively small but suggest that upon binding of ADP the protein becomes more compact and exposes a reduced protein surface area to the aqueous solvent, whereas in the AMP-PNP-bound state, no changes in solvent accessible area occur (see Discussion).

In contrast to ADP and AMP-PNP binding, large differences are expected for the ITC diagrams of the binding of ATP to wt and mutant GlcV proteins. Since each titration of the E166A mutant with ATP will include not only ATP binding but also ATP hydrolysis and NBD dimerization, such titrations are difficult to analyze and are therefore not further described here. Figure 6A shows typical ATP titration curves for wt GlcV and the G144A mutant at 60 °C in the presence of Mg^{2+}. The nucleotide binding stoichiometry was close to 1 for both proteins (see Table 2). Remarkably, when the ITC diagrams of wt GlcV and the G144A mutant were compared, a constant enthalpic component (compared to G144A) was observed for wt GlcV for every injection. This constant enthalpic contribution remained after saturation of the proteins with nucleotide and subtraction of the nucleotide dilution effect (Figure 6A). When the ITC data of wt GlcV were corrected for the ATP dilution effect and for the observed constant enthalpic contribution ($\Delta H_{constant}$), values for ΔH, ΔG, and $-T\Delta S$ of the remaining curve were calculated (see Table 2). The obtained values at the different temperatures were remarkably similar to those observed for binding of ADP to wt GlcV and exhibit a dependence similar to that of ADP binding, which indicates that the titration curves of wt GlcV with ATP consist of the sum of a constant component ($\Delta H_{constant}$ in Table 2) and a component attributable to ADP binding ($\Delta H_{binding}$ in Table 2). Because no signal was observed for the G144A protein after substraction of the ATP dilution effect at higher ATP:NBS stoichiometries and because no ATP hydrolysis occurs with this mutant, we can attribute the constant component observed with wt GlcV under these conditions to ATP hydrolysis. Since G144 is not located in the binding site of the monomeric NBD, we propose that the ITC profile of binding of Mg^{2+}-ATP to the G144A mutant corresponds to the ATP binding reaction to monomeric GlcV.

Thermodynamics of Nucleotide-Induced Dimerization of GlcV. To determine the thermodynamics of dimerization of GlcV, ITC curves for binding of ATP to the G144A and E166A mutants in the presence of EDTA were determined. Under these conditions, no hydrolysis of ATP takes place (Figure 2A), whereas the E166A mutant forms a stable dimer (Figure 1B). Figure 7A shows a typical ATP titration curve

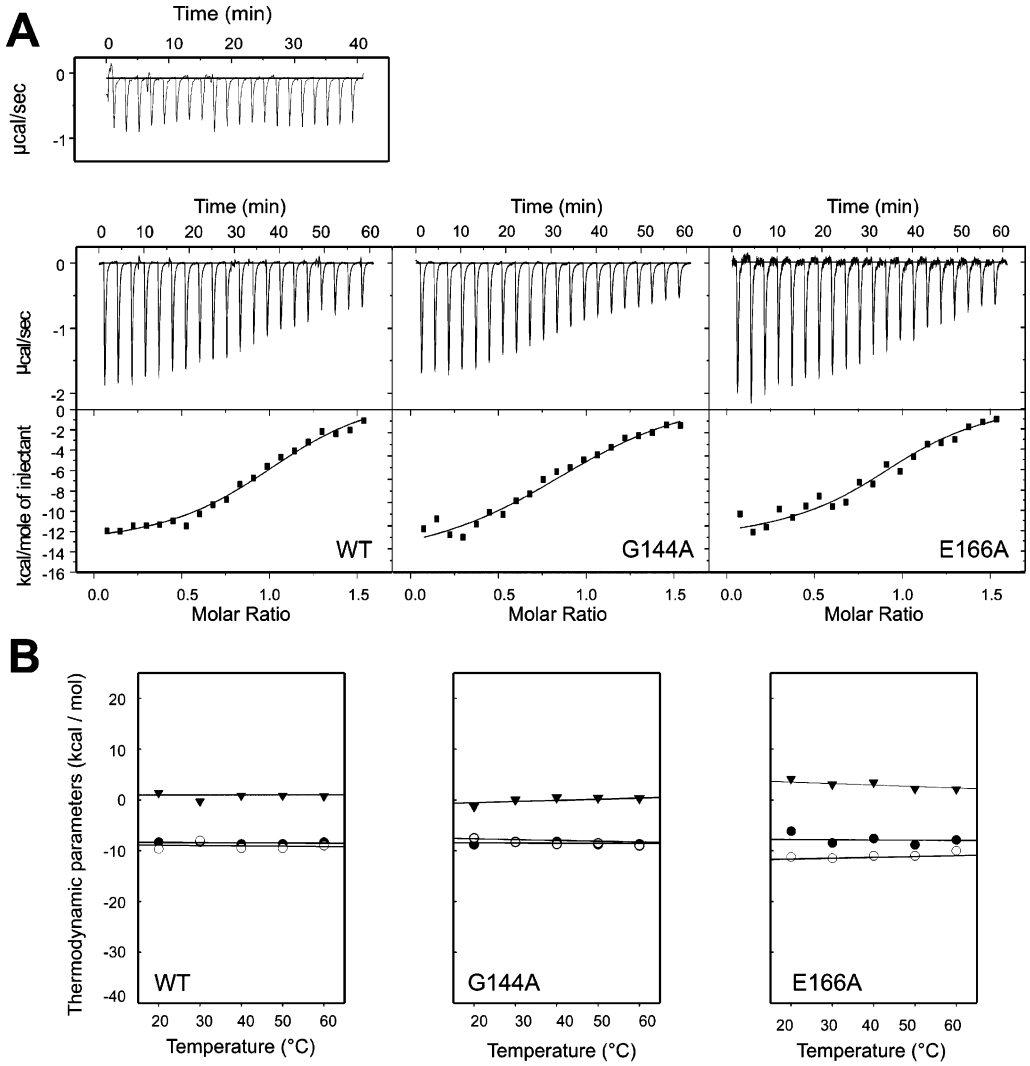

FIGURE 5: Isothermal titration calorimetry of binding of Mg^{2+}-AMP-PNP to wt GlcV and the G144A and E166A mutants. (A) The top panel depicts the dilution effect of the titration of Mg^{2+}-AMP-PNP at 40 °C. The middle panel depicts the binding isotherm for the titration of wt GlcV and the G144A and E166A mutants with Mg^{2+}-AMP-PNP at 40 °C. Twenty injections of 5 μL of a 600 μM nucleotide solution were made at 180 s intervals in a volume of 2.1 mL containing 30 μM protein. The area under each injection signal was integrated, and in the bottom panel, the enthalpy per mole of nucleotide injected is plotted vs the nucleotide:NBD molar ratio. The solid line represents a nonlinear least-squares fit of the reaction heat for the injection. (B) Temperature dependence of the thermodynamic parameters of Mg^{2+}-AMP-PNP binding from 20 to 60 °C: (○) ΔH, (●) ΔG, and (▼) $-T\Delta S$.

Table 1: Thermodynamic Parameters, Nucleotide Binding Stoichiometries, and Affinities for wt and Mutant GlcV in the Presence of Mg^{2+}

		ADP-Mg^{2+}					AMP-PNP-Mg^{2+}				
GlcV protein	temp (°C)	ΔG (kcal/mol)	ΔH (kcal/mol)	$-T\Delta S$ (kcal/mol)	n	K_d (nM)	ΔG (kcal/mol)	ΔH (kcal/mol)	$-T\Delta S$ (kcal/mol)	n	K_d (μM)
wt	20	-10.6 ± 0.0	-13.0 ± 0.9	2.4 ± 0.9	0.91 ± 0.05	12.5 ± 0.5	-8.3 ± 0.5	-9.7 ± 0.5	1.4 ± 1.0	0.99 ± 0.05	0.7 ± 0.07
	30	-10.1 ± 0.1	-14.5 ± 1.3	4.5 ± 1.4	0.91 ± 0.04	55 ± 2.5	-8.3 ± 0.9	-8.0 ± 1.1	-0.3 ± 1.8	0.91 ± 0.02	1.0 ± 0.05
	40	-10.4 ± 0.8	-16.5 ± 0.9	6.1 ± 1.7	0.91 ± 0.02	55 ± 4.3	-8.7 ± 0.4	-9.5 ± 1.0	0.8 ± 1.4	0.91 ± 0.04	0.9 ± 0.0
	50	-10.4 ± 1.1	-18.3 ± 0.7	7.9 ± 1.8	0.91 ± 0.02	100 ± 5.3	-8.6 ± 0.4	-9.5 ± 0.08	0.9 ± 1.2	0.87 ± 0.05	1.5 ± 0.45
	60	-9.7 ± 0.9	-19.5 ± 1.3	9.8 ± 2.2	0.91 ± 0.02	450 ± 10.5	-8.3 ± 0.5	-9.0 ± 0.6	0.7 ± 1.1	0.91 ± 0.05	3.6 ± 0.67
G144A	20	-10.4 ± 0.8	-13.8 ± 0.5	3.5 ± 1.3	0.84 ± 0.02	20 ± 2.0	-8.8 ± 0.3	-7.5 ± 0.0	-1.3 ± 0.3	0.90 ± 0.1	0.3 ± 0.025
	30	-9.9 ± 0.9	-15.6 ± 0.9	5.7 ± 1.8	0.84 ± 0.02	72 ± 14	-8.2 ± 0.3	-8.3 ± 0.0	0.1 ± 0.3	0.76 ± 0.05	1.2 ± 0.05
	40	-9.9 ± 0.5	-17.5 ± 1.2	7.6 ± 1.7	0.83 ± 0.04	120 ± 16	-8.2 ± 0.3	-8.7 ± 0.1	0.5 ± 0.4	0.80 ± 0.12	1.8 ± 0.0
	50	-10.4 ± 0.5	-17.8 ± 0.8	7.4 ± 1.3	0.83 ± 0.02	110 ± 16	-8.1 ± 0.4	-8.5 ± 0.1	0.4 ± 0.5	0.86 ± 0.06	3.3 ± 0.7
	60	-10.3 ± 0.6	-18.5 ± 0.6	8.2 ± 1.2	0.80 ± 0.05	170 ± 9.0	-8.7 ± 0.4	-9.0 ± 0.5	0.3 ± 0.9	0.60 ± 0.05	2.0 ± 1.05
E166A	20	-9.9 ± 0.3	-14.5 ± 0.9	4.6 ± 1.1	0.73 ± 0.08	40 ± 1.5	-6.0 ± 0.0	-11.9 ± 0.0	6.0 ± 0.1	0.94 ± 0.07	0.5 ± 0.02
	30	-9.5 ± 0.2	-16.6 ± 0.7	7.0 ± 0.9	0.71 ± 0.07	140 ± 3.2	-8.5 ± 0.3	-11.5 ± 0.0	3.3 ± 0.3	1.02 ± 0.02	0.8 ± 0.02
	40	9.4 ± 0.0	-17.5 ± 0.7	8.0 ± 0.7	0.68 ± 0.05	260 ± 5.5	-7.6 ± 0.1	-12.0 ± 0.0	4.4 ± 0.1	0.95 ± 0.05	5.0 ± 1.0
	50	-9.3 ± 0.8	-18.0 ± 0.6	8.6 ± 1.4	0.83 ± 0.05	500 ± 11	-8.8 ± 0.3	-11.0 ± 0.2	2.2 ± 0.5	0.99 ± 0.03	1.1 ± 1.2
	60	-9.0 ± 0.9	-18.5 ± 0.6	9.5 ± 1.5	0.83 ± 0.04	1250 ± 23	-7.9 ± 0.5	-10.0 ± 0.2	2.0 ± 0.7	0.86 ± 0.03	6.6 ± 0.8

for G144A and E166A GlcV at 40 °C, and Figure 7B shows the ΔG, ΔH, and $-T\Delta S$ values as a function of the temperature. Both the ΔH values and ATP binding affinities (Table 3) were lower in the absence of Mg^{2+} and more similar to those observed for AMP-PNP binding. This demonstrates that Mg^{2+} has a large effect on both the affinity

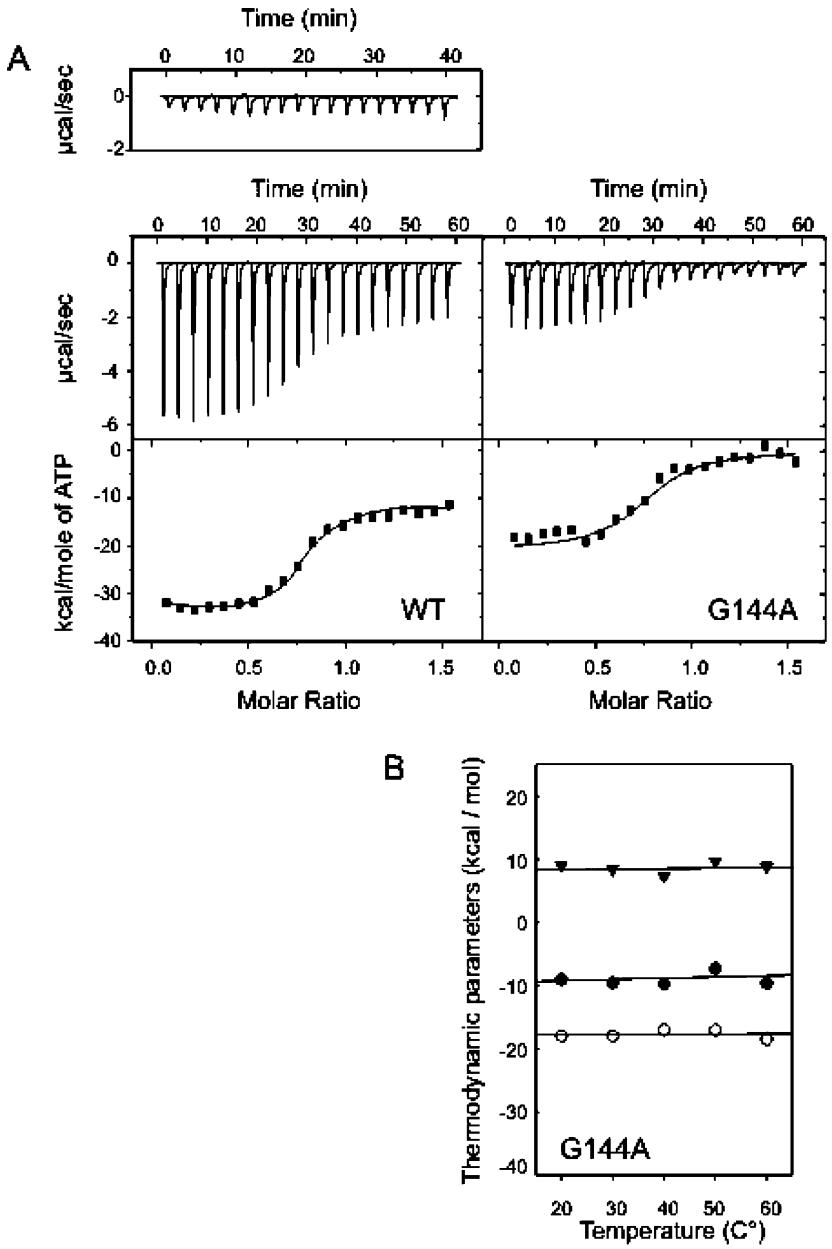

FIGURE 6: Isothermal titration calorimetry of binding of Mg^{2+}-ATP to wt GlcV and the G144A mutant. (A) The top panel depicts the dilution effect of the titration of Mg^{2+}-ATP at 60 °C. The middle panel depicts the binding isotherm for the titration of wt GlcV and the G144A mutant with Mg^{2+}-ATP at 60 °C. Twenty injections of 5 μL of a 600 μM nucleotide solution were made at 180 s intervals in a volume of 2.1 mL containing 30 μM proteins. The area under each injection signal was integrated, and in the bottom panel, the enthalpy per mole of nucleotide injected is plotted vs the nucleotide:NBD molar ratio. The solid line represents a nonlinear least-squares fit of the reaction heat for the injection. (B) Temperature dependence of thermodynamic parameters for binding of Mg^{2+}-ATP to the G144A mutant from 20 to 60 °C. The G144A mutant represents the thermodynamics of binding of ATP to the NBD: (○) ΔH, (●) ΔG, and (▼) $-T\Delta S$.

and entropy of nucleotide binding. Although the ΔG values are comparable for the two mutants, ΔH and $-T\Delta S$ values differed as well as their temperature dependence. The binding enthalpy for the G144A mutant showed a negative ΔC_p of -102.5 cal mol^{-1} K^{-1}, while the E166A mutant showed a positive ΔC_p of 111.7 cal mol^{-1} K^{-1}. Remarkably, both the G144A and E166A mutants gave binding stoichiometries of ~1. Since in E166A, the dimer is formed, this further demonstrates that the E166A dimer contains two nucleotides. Since the G144A and E166A mutants behaved very similarly in binding of ADP and AMP-PNP, and since both mutants were unable to hydrolyze ATP in the absence of Mg^{2+}, we conclude that the difference between the two mutants is caused by the dimerization reaction. Therefore, the ΔH and $-T\Delta S$ of dimerization can be calculated from the difference in ΔG, ΔH, and $-T\Delta S$ between the G144A and E166A mutants. The ΔG, ΔH, and $-T\Delta S$ of dimerization changed with temperature, ranging from -1, -5.6, and 4.6 kcal/mol of dimer formed at 20 °C to -3, 11.6, and -14.6 kcal/mol of dimer formed at 60 °C, respectively. We therefore conclude that dimerization of the E166A mutant at the lower temperatures is driven by enthalpic contributions, while at higher temperatures, the entropic contributions dominate. The latter is most likely due to the exclusion of water molecules from the protein surface that is involved in dimer formation.

Table 2: Thermodynamic Parameters for Binding of ATP to wt GlcV in the Presence of Mg^{2+}

GlcV protein	temp (°C)	$\Delta H_{constant}$[a] (kcal/mol)	$\Delta G_{binding}$[b] (kcal/mol)	$\Delta H_{binding}$[b] (kcal/mol)	$-T\Delta S_{binding}$[b] (kcal/mol)	*n*	K_d (nM)
wt	20	−5.0 ± 0.1	−9.7 ± 0.1	−16.0 ± 0.3	6.3 ± 0.4	0.79 ± 0.01	50 ± 4.5
	30	−8.5 ± 0.1	−10.1 ± 0.5	−17.0 ± 0.4	6.9 ± 0.9	0.81 ± 0.00	52 ± 3.3
	40	−9.0 ± 0.05	−10.2 ± 0.0	−18.5 ± 0.5	8.3 ± 0.5	0.77 ± 0.05	78 ± 4.0
	50	−10.0 ± 0.2	−10.1 ± 0.0	−20.0 ± 0.8	9.9 ± 0.8	0.79 ± 0.05	155 ± 3.5
	60	−12.5 ± 0.1	−9.8 ± 0.5	−21.0 ± 0.3	11.2 ± 0.80	0.76 ± 0.02	350 ± 5.0
G144A	20		−9.0 ± 0.3	−18.0 ± 0.9	9.0 ± 1.2	0.75 ± 0.05	20 ± 1.0
	30		−9.6 ± 0.8	−18.0 ± 0.8	8.4 ± 1.6	0.76 ± 0.03	125 ± 1.5
	40		−9.7 ± 0.6	−17.0 ± 1.3	7.3 ± 1.9	0.76 ± 0.03	160 ± 4.0
	50		−7.3 ± 1.3	−17.0 ± 0.1	9.7 ± 1.4	0.76 ± 0.03	120 ± 8.5
	60		−9.6 ± 0.5	−18.5 ± 0.1	8.9 ± 0.6	0.76 ± 0.05	500 ± 7.3

[a] The ΔH of ATP hydrolysis. [b] The ΔH of ADP binding.

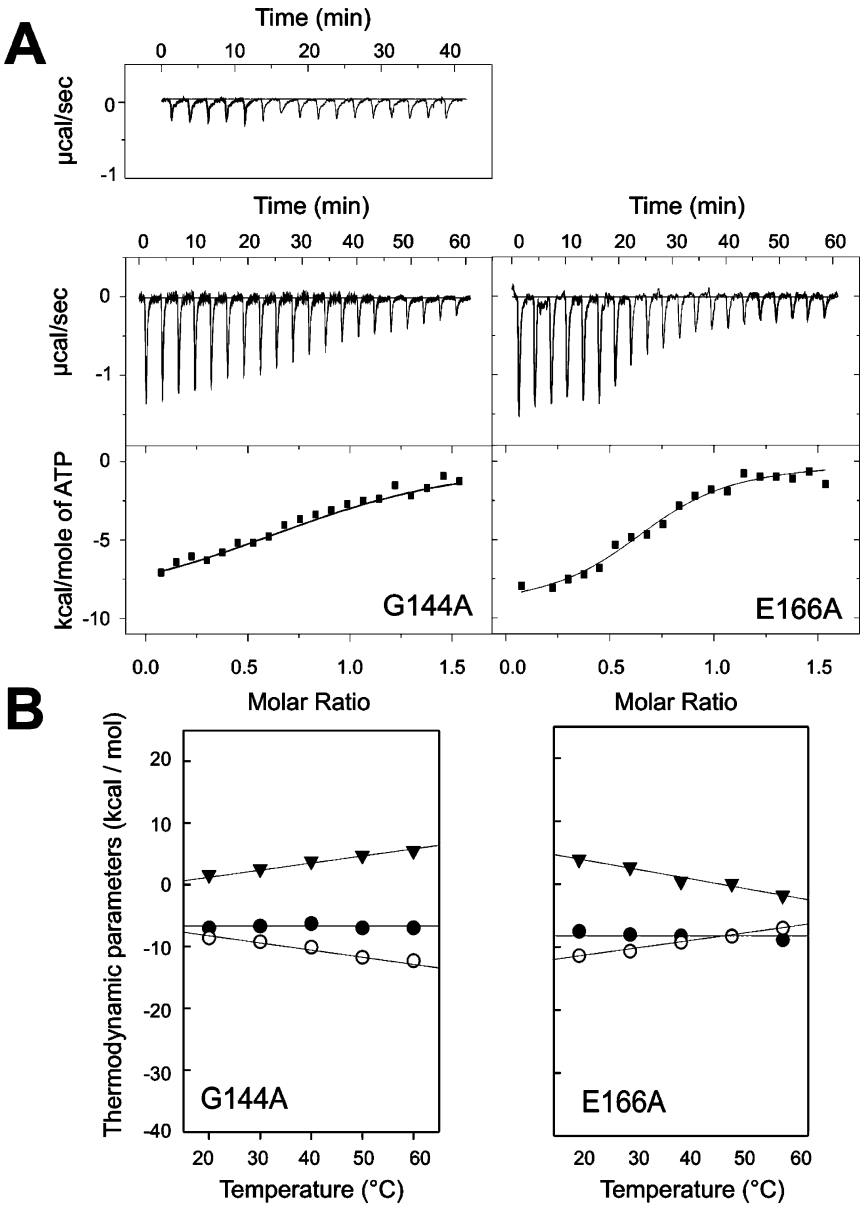

FIGURE 7: Isothermal titration calorimetry of binding of ATP to the G144A and E166A mutants in the absence of magnesium. (A) The top panel depicts the dilution effect of the titration of ATP at 40 °C. The middle panel depicts the binding isotherm for the titration of the G144A and E166A mutants with ATP at 40 °C. Twenty injections of 5 μL of a 600 μM nucleotide solution were made at 180 s intervals in a volume of 2.1 mL containing 30 μM GlcV. The area under each injection signal was integrated, and in the bottom panel, the enthalpy per mole of nucleotide injected is plotted vs the nucleotide:NBD molar ratio. The solid line represents a nonlinear least-squares fit of the reaction heat for the injection. (B) Temperature dependence of the thermodynamic parameters of ATP binding from 20 to 60 °C: (○) ΔH, (●) ΔG, and (▼) $-T\Delta S$.

DISCUSSION

In the past decade, the mechanism of ATP-dependent transport by ABC transporters has been studied extensively using genetic, biochemical, and structural approaches (*2*−*5*, *30*−*32*). Crystal structures and biochemical data have

Table 3: Thermodynamic and Kinetic Parameters for Binding of ATP to Mutant GlcV Proteins in the Absence of Mg^{2+}

GlcV mutant	temp (°C)	ΔG (kcal/mol)	ΔH (kcal/mol)	$-T\Delta S$ (kcal/mol)	n	K_d (μM)
G144A	20	-7.0 ± 0.4	-8.6 ± 0.0	1.6 ± 0.4	0.82 ± 0.15	2.5 ± 0.7
	30	-6.7 ± 0.2	-9.2 ± 0.1	2.5 ± 0.3	0.93 ± 0.00	4.3 ± 0.5
	40	-6.2 ± 0.0	-10.1 ± 0.1	3.8 ± 0.1	0.95 ± 0.00	9.5 ± 0.2
	50	-7.0 ± 0.1	-11.7 ± 0.0	4.7 ± 0.1	0.70 ± 0.06	6.1 ± 0.05
	60	-7.3 ± 0.1	-12.8 ± 0.3	5.4 ± 0.4	0.75 ± 0.05	5.3 ± 0.05
E166A	20	-7.5 ± 0.7	-11.4 ± 0.3	3.9 ± 1.0	0.72 ± 0.03	2.5 ± 0.05
	30	-8.0 ± 0.1	-10.7 ± 0.1	2.6 ± 0.2	0.70 ± 0.05	1.6 ± 0.2
	40	-8.3 ± 0.2	-8.6 ± 0.0	0.39 ± 0.2	0.75 ± 0.02	1.7 ± 0.2
	50	-8.3 ± 0.3	-8.3 ± 0.0	0.05 ± 0.3	0.99 ± 0.05	2.6 ± 1.5
	60	-8.8 ± 0.3	-7.0 ± 0.1	-1.8 ± 0.4	0.85 ± 0.10	1.5 ± 2.1

deepened our understanding of these processes, although the exact mechanism of the coupling between transport and ATP hydrolysis remains a topic of debate. Thermodynamic studies can provide detailed insights into the coupling mechanism and in particular into the conformational changes that are associated with nucleotide binding and hydrolysis. GlcV is the NBD of the glucose ABC transporter of the hyperthermoacidophile *S. solfataricus*. It has been characterized both biochemically and structurally (*19*, *20*, *23*, *24*). GlcV, the ATPase subunit of the glucose transporter, is highly thermostable over a wide range of temperatures and therefore an excellent candidate for thermodynamic studies. The ATPase cycle of the NBD is believed to involve several distinct steps, namely, ATP binding, NBD dimerization, ATP hydrolysis, and subsequent dissociation of the dimer and release of the bound ADP. Here we have used mutants of GlcV that are arrested at specific steps in this cycle. The wild-type GlcV protein immediately hydrolyzes the ATP to ADP. Therefore, the nonhydrolyzable ATP analogue AMP-PNP, which is often suggested to mimic ATP binding, was used. It should be noted that AMP-PNP was shown not to induce dimerization (*16*) and therefore does not completely mimic ATP binding. Our data show that a mutant of GlcV, G144A, still binds ATP with high affinity but that it is unable to hydrolyze ATP. This mutant no longer dimerizes (Figure 1B) and thus represents an intermediate in which binding of a nucleotide to the monomeric NBD can be analyzed in a manner independent of the dimerization step. Furthermore, also a mutant was used that still dimerizes but that is unable to hydrolyze ATP. The E166A mutant was previously described as a mutant which shows a Mg^{2+}- and ATP-dependent dimerization with a strongly reduced ATPase activity (*23*). However, the protein could only be trapped in a dimeric form at a high ATP concentration as evidenced by size-exclusion chromatography, suggesting that the dimer is unstable on the column (*23*). Remarkably, the presence of glycerol destabilized the dimeric species. We now report that this mutant forms stable dimers at low ATP concentrations in the absence of glycerol and Mg^{2+}. Indeed, it was previously shown that the ATP hydrolysis of several NBDs, e.g., HisP (*33*) and Mdl1 (C. van der Does and R. Tampé, unpublished data), is inhibited by glycerol. Moreover, studies on protein and solvent dynamics suggest that compounds such as glycerol can control the solvent dynamics of proteins and affect their activity by forming rigid structures that increase the energy barriers for conformational fluctuations of proteins (*34*). We also noticed that the E166A mutant is not completely arrested in ATP hydrolysis, but that its activity is decreased 100-fold as compared to that of wt GlcV. Analysis of the activation enthalpies ($\Delta H^{\ddagger}$) for ATP hydrolysis by the wt and E166A mutant showed rather similar activation enthalpies. Larger differences were observed for the free activation enthalpy, and the free activation entropy indicated that the enthalpy change to reach the transition state is approximately similar for the wt and E166A mutant; however, the lower reaction rate of the E166A mutant is a result of the more positive $-T\Delta S^{\ddagger}$ of its transition state. This suggests that the transition state of the E166A mutant has a more ordered or more rigid structure than the transition state of the wt protein. Since the ATPase activity complicates the analysis of the ITC experiments, we sought conditions that result in a complete block of the ATPase activity without affecting ATP-dependent dimerization. In the absence of Mg^{2+}, the ATPase activity of this mutant is negligible (Figure 2C) while the protein still forms stable dimers (Figure 1B). With these optimized conditions, the wt and the two mutant proteins enabled us to determine thermodynamic parameters of different steps of the ATP hydrolysis cycle.

As expected, the ITC data demonstrate that the nucleotides bind to GlcV and the two mutants in a nearly stoichiometric fashion. This implies that the monomer binds a single ATP molecule and that 90% or more of the isolated and purified protein is active in ATP binding. ATP and ADP bind with a comparable high affinity, while AMP-PNP binds with a 100-fold reduced affinity. Likewise, in the absence of Mg^{2+}, ATP also was found to bind with a reduced affinity (see K_d values in Tables 2 and 3). Furthermore, the ΔG, ΔH, and $-T\Delta S$ values were much smaller for Mg^{2+}-AMP-PNP (Figure 5) or ATP in the absence of Mg^{2+} (Figure 7) than for Mg^{2+}-ATP (Figure 6) or Mg^{2+}-ADP (Figure 4). In the Mg^{2+}-ADP GlcV structure, the nucleotide has several contacts with the Mg^{2+} ion. Mg^{2+} stabilizes the binding of the nucleotide, resulting in a large change in enthalpy, which compensates the decrease in entropy upon Mg^{2+} binding (see Table 3). Compared to the Mg^{2+}-ADP structure, the Mg^{2+}-AMP-PNP structure shows several extra hydrogen bonds with the γ-phosphate and the nitrogen between the β- and γ-phosphates, but also changes in the coordination of the Mg^{2+} (*20*). On the basis of the crystal structures of GlcV, the lack of or improper coordination of Mg^{2+} results in a reduced binding affinity of ATP in the absence of Mg^{2+} or Mg^{2+}-AMP-PNP. In our experiment, we also observed that the nucleotide binding affinity strongly decreases with temperature. At temperatures close to the growth temperature of *S. solfataricus*, the nucleotide binding affinity of GlcV is comparable to what has been observed for the NBDs of other ABC transporters, i.e., values in the micromolar range (*15*,

27, *28*, *33*). However, at low temperatures, the nucleotides bind with nanomolar affinity.

The measured values of ΔH, ΔG, and $-T\Delta S$ for ADP and AMP-PNP binding and their temperature dependence were similar for wt GlcV and the G144A mutant, indicating that this mutation does not influence nucleotide binding. Indeed, glycine 144 is not localized in the nucleotide-binding site of the monomer. Comparison with the dimeric structures shows, however, that in the dimer this residue contacts the γ-phosphate of the nucleotide bound to the opposite dimer (*6*, *8*−*10*). This contact seems important for dimer formation, and the complete lack of ATPase activity (Figure 2A) upon mutagenesis of this residue shows the importance of dimer formation for ATP hydrolysis. The E166A mutant exhibited a slightly reduced nucleotide binding affinity. Although glutamate 166 does not directly contact the nucleotide, in the HlyB structure, it coordinates a water molecule, which coordinates the γ-phosphate and a water molecule, which forms the octrahedral coordination sphere of Mg^{2+} (*6*). This contact thus likely contributes to the stability of the bound nucleotide. Indeed, the presence of Mg^{2+} had a strong effect on binding of nucleotides. Binding of the nucleotides was driven with a large negative ΔH and opposed by a positive $-T\Delta S$. While the binding enthalpy for Mg^{2+}-ATP and Mg^{2+}-AMP-PNP of the G144A mutant was temperature-independent, Mg^{2+}-ADP binding exhibited a strong temperature dependence. The ΔC_p for binding of Mg^{2+}-ADP to the wt, G144A, and E166A GlcV proteins was −167.5, −115.4, and −94.5 cal mol^{-1} K^{-1}, respectively. In ligand binding experiments, a strong correlation exists between ΔC_p and the buried surface area (*35*, *36*). A large negative ΔC_p suggests a reduced level of exposure of the protein surface area to aqueous solvent (*37*). Analysis of the nucleotide-bound and free states of crystal structures of various NBDs indicated only minor structural changes between the ADP-bound and nucleotide-free state. However, when ATP binds, a large rigid body movement occurs. Remarkably, in the crystal structure of GlcV, conformational differences were found between the nucleotide-free and the more rigid Mg^{2+}-AMP-PNP- and Mg^{2+}-ADP-bound states, whereas the comparison between the Mg^{2+}-AMP-PNP and Mg^{2+}-ADP structures showed only minor differences (*20*). Compared to the changes in ΔC_p found for other protein−ligand interactions, e.g., −780 cal mol^{-1} K^{-1} for *Bacillus subtilis* SecA (*38*) and −330 kcal mol^{-1} K^{-1} for native myosin (*39*), the ΔC_p value observed when ADP binds to GlcV is relatively small. This supports the notion that either the changes in solvent accessibility upon nucleotide binding are small or the increase in solvent accessible area in one area is compensated by a decrease in solvent accessible area in another region.

Vanadate trapping experiments with several complete transporters, like P-glycoprotein (P-gp) (*12*, *40*) and the maltose transporter of *E. coli* $MalFGK_2$ (*13*), indicated the presence of only one nucleotide in the NBD dimer and led to the alternating site (*12*) model for ATP hydrolysis. Our DLS and ITC experiments indicate, however, that the dimer contains two nucleotides, confirming previous structural information about NBD dimers (*6*, *8*−*10*). Moreover, previous size-exclusion experiments with E166Q GlcV (*23*) and analysis of the nucleotide composition of three trapped intermediate states of the NBD of Mdl1p, a mitochondrial peptide ABC transporter (*15*), also indicated a stoichiometry of two nucleotides per dimer. These data have led to the processive clamp model for ATP hydrolysis in which two nucleotides are bound to the NBD which are hydrolyzed in a processive manner (*15*). Since in this study we also find a stoichiometry of two nucleotides per dimer, we will here discuss the thermodynamics of ATP hydrolysis based on this processive clamp model. Our data show that the first step in the ATP hydrolysis cycle, ATP binding, is an energetically favorable step, which is driven by a negative ΔH and opposed by a positive $-T\Delta S$. The second step, dimerization of ATP-bound NBD, is in the E166A GlcV also an energetically favorable process, which is driven at low temperatures by enthalpy and at higher temperatures by entropy. We propose that the dimerization in wt GlcV behaves like the dimerization of E166A GlcV. The ΔG of ATP hydrolysis was determined to be in the range of −7 to −9 kcal/mol. ATP hydrolysis is a favorable step, driven by both a negative ΔH and $-T\Delta S$. Since no stable dimers of the NBDs of ABC transporters are formed in the presence of ADP (*20*, *41*−*43*) and the ADP-bound dimers could be isolated only when the system was stabilized by BeF_x trapping (*15*), dissociation of the NBD dimer after hydrolysis of both ATP molecules most likely also is an energetically favorable step. This result fits well with the recently determined crystal structure of ADP-Mg^{2+}-bound MalK, the closest homologue of GlcV, where the dimer in the posthydrolytic state is reset to the open state (*11*). Whether dissociation of the ATP/ADP-bound state is favorable may depend on the NBD that is studied. Therefore, only the final step in the cycle, dissociation of ADP from the NBD, is an energetically unfavorable process. The energy requirement of this step is, however, compensated by the more favorable binding of ATP in a next round, and the higher ATP concentration in the cell. Here we have determined the thermodynamics of different steps of the ATP hydrolysis cycle of an isolated NBD. Future studies should determine the thermodynamics with the full-length transporter, in an effort to assess whether the interaction between the NBDs and MSDs influences the thermodynamic pathway. Although the determination of this pathway in full-length proteins will be a challenging task, it will provide detailed insight into the mechanism of energy conversion in ABC transporters and how this is coupled to the movement of the transported substrate.

ACKNOWLEDGMENT

We thank Andy-Mark Thunnissen, Gregory Verdon, and Cyril Hamiaux for helpful discussions and assistance with the size-exclusion and dynamic light scattering measurements, Bert Poolman for the use of the isothermal titration calorimeter, and Lutz Schmitt and Laszlo Csanady for many helpful comments on the manuscript.

REFERENCES

1. Higgins, C. F. (1992) ABC transporters: From microorganisms to man, *Annu. Rev. Cell Biol. 8*, 67−113.
2. Davidson, A. L., and Chen, J. (2004) ATP-binding cassette transporters in bacteria, *Annu. Rev. Biochem. 73*, 241−268.
3. Higgins, C. F., and Linton, K. J. (2004) The ATP switch model for ABC transporters, *Nat. Struct. Mol. Biol. 11*, 918−926.
4. Locher, K. P. (2004) Structure and mechanism of ABC transporters, *Curr. Opin. Struct. Biol. 14*, 426−431.

5. van der Does, C., and Tampé, R. (2004) How do ABC transporters drive transport? *Biol. Chem. 385*, 927−933.
6. Zaitseva, J., Jenewein, S., Jumpertz, T., Holland, I. B., and Schmitt, L. (2005) H662 is the linchpin of ATP hydrolysis in the nucleotide-binding domain of the ABC transporter HlyB, *EMBO J. 24*, 1901−1910.
7. Jones, P. M., and George, A. M. (1999) Subunit interactions in ABC transporters: Towards a functional architecture, *FEMS Microbiol. Lett. 179*, 187−202.
8. Hopfner, K. P., Karcher, A., Shin, D. S., Craig, L., Arthur, L. M., Carney, J. P., and Tainer, J. A. (2000) Structural biology of Rad50 ATPase: ATP-driven conformational control in DNA double-strand break repair and the ABC-ATPase superfamily, *Cell 101*, 789−800.
9. Smith, P. C., Karpowich, N., Millen, L., Moody, J. E., Rosen, J., Thomas, P. J., and Hunt, J. F. (2002) ATP binding to the motor domain from an ABC transporter drives formation of a nucleotide sandwich dimer, *Mol. Cell 10*, 139−149.
10. Chen, J., Lu, G., Lin, J., Davidson, A. L., and Quiocho, F. A. (2003) A tweezers-like motion of the ATP-binding cassette dimer in an ABC transport cycle, *Mol. Cell 12*, 651−661.
11. Lu, G., Westbrooks, J. M., Davidson, A. L., and Chen, J. (2005) ATP hydrolysis is required to reset the ATP-binding cassette dimer into the resting-state conformation, *Proc. Natl. Acad. Sci. U.S.A. 102*, 17969−17974.
12. Senior, A. E., al Shawi, M. K., and Urbatsch, I. L. (1995) The catalytic cycle of P-glycoprotein, *FEBS Lett. 377*, 285−289.
13. Sharma, S., and Davidson, A. L. (2000) Vanadate-induced trapping of nucleotides by purified maltose transport complex requires ATP hydrolysis, *J. Bacteriol. 182*, 6570−6576.
14. Urbatsch, I. L., Tyndall, G. A., Tombline, G., and Senior, A. E. (2003) P-Glycoprotein catalytic mechanism: Studies of the ADP-vanadate inhibited state, *J. Biol. Chem. 278*, 23171−23179.
15. Janas, E., Hofacker, M., Chen, M., Gompf, S., Van der Does, C., and Tampé, R. (2003) The ATP hydrolysis cycle of the nucleotide-binding domain of the mitochondrial ATP-binding cassette transporter Mdl1p, *J. Biol. Chem. 278*, 26862−26869.
16. Moody, J. E., Millen, L., Binns, D., Hunt, J. F., and Thomas, P. J. (2002) Cooperative, ATP-dependent association of the nucleotide binding cassettes during the catalytic cycle of ATP-binding cassette transporters, *J. Biol. Chem. 277*, 21111−21114.
17. van der Does, C., Presenti, C., Schulze, K., Dinkelaker, S., and Tampé, R. (2005) Kinetics of the ATP hydrolysis cycle of the nucleotide-binding domain of MDL1 studied by a novel site-specific labeling technique, *J. Biol. Chem. 281*, 5694−5701.
18. al-Shawi, M. K., Figler, R. A., Omote, H., and Polar, M. K. (2003) Transition state analysis of the coupling of drug transport to ATP hydrolysis by P-glycoprotein, *J. Biol. Chem. 278*, 52629−52640.
19. Albers, S. V., Elferink, M. G., Charlebois, R. L., Sensen, C. W., Driessen, A. J. M., and Konings, W. N. (1999) Glucose transport in the extremely thermoacidophilic *Sulfolobus solfataricus* involves a high-affinity membrane-integrated binding protein, *J. Bacteriol. 181*, 4285−4291.
20. Verdon, G., Albers, S. V., Dijkstra, B. W., Driessen, A. J. M., and Thunnissen, A. M. (2003) Crystal structures of the ATPase subunit of the glucose ABC transporter from *Sulfolobus solfataricus*: Nucleotide-free and nucleotide-bound conformations, *J. Mol. Biol. 330*, 343−358.
21. Panagiotidis, C. H., Boos, W., and Shuman, H. A. (1998) The ATP-binding cassette subunit of the maltose transporter MalK antagonizes MalT, the activator of the *Escherichia coli* mal regulon, *Mol. Microbiol. 30*, 535−546.
22. Bohm, A., Diez, J., Diederichs, K., Welte, W., and Boos, W. (2002) Structural model of MalK, the ABC subunit of the maltose transporter of *Escherichia coli*: Implications for mal gene regulation, inducer exclusion, and subunit assembly, *J. Biol. Chem. 277*, 3708−3717.
23. Verdon, G., Albers, S. V., van Oosterwijk, N., Dijkstra, B. W., Driessen, A. J. M., and Thunnissen, A. M. (2003) Formation of the productive ATP-Mg^{2+}-bound dimer of GlcV, an ABC-ATPase from *Sulfolobus solfataricus*, *J. Mol. Biol. 334*, 255−267.
24. Verdon, G., Albers, S. V., Dijkstra, B. W., Driessen, A. J. M., and Thunnissen, A. M. (2002) Purification, crystallization and preliminary X-ray diffraction analysis of an archaeal ABC-ATPase, *Acta Crystallogr. D58*, 362−365.
25. Garcia De La, T. J., Huertas, M. L., and Carrasco, B. (2000) Calculation of hydrodynamic properties of globular proteins from their atomic-level structure, *Biophys. J. 78*, 719−730.
26. Wiseman, T., Williston, S., Brandts, J. F., and Lin, L. N. (1989) Rapid measurement of binding constants and heats of binding using a new titration calorimeter, *Anal. Biochem. 179*, 131−137.
27. Zaitseva, J., Jenewein, S., Wiedenmann, A., Benabdelhak, H., Holland, I. B., and Schmitt, L. (2005) Functional characterization and ATP-induced dimerization of the isolated ABC-domain of the haemolysin B transporter, *Biochemistry 44*, 9680−9690.
28. Horn, C., Bremer, E., and Schmitt, L. (2003) Nucleotide dependent monomer/dimer equilibrium of OpuAA, the nucleotide-binding protein of the osmotically regulated ABC transporter OpuA from *Bacillus subtilis*, *J. Mol. Biol. 334*, 403−419.
29. Liu, R., and Sharom, F. J. (1997) Fluorescence studies on the nucleotide binding domains of the P-glycoprotein multidrug transporter, *Biochemistry 36*, 2836−2843.
30. Austermuhle, M. I., Hall, J. A., Klug, C. S., and Davidson, A. L. (2004) Maltose binding protein is open in the catalytic transition state for ATP hydrolysis during maltose transport, *J. Biol. Chem. 279*, 28243−28250.
31. Schmitt, L., and Tampé, R. (2002) Structure and mechanism of ABC transporters, *Curr. Opin. Struct. Biol. 12*, 754−760.
32. Jones, P. M., and George, A. M. (2004) The ABC transporter structure and mechanism: Perspectives on recent research, *Cell. Mol. Life Sci. 61*, 682−699.
33. Nikaido, K., Liu, P. Q., and Ames, G. F. (1997) Purification and characterization of HisP, the ATP-binding subunit of a traffic ATPase (ABC transporter), the histidine permease of *Salmonella typhimurium.* Solubility, dimerization, and ATPase activity, *J. Biol. Chem. 272*, 27745−27752.
34. Caliskan, G., Mechtani, D., Roh, J. H., Kisliuk, A., Sokolov, A. P., Azzam, S., Cicerone, M. T., Lin-Gibson, S., and Peral, I. (2004) Protein and solvent dynamics: How strongly are they coupled? *J. Chem. Phys. 121*, 1978−1983.
35. Livingstone, J. R., Spolar, R. S., and Record, M. T., Jr. (1991) Contribution to the thermodynamics of protein folding from the reduction in water-accessible nonpolar surface area, *Biochemistry 30*, 4237−4244.
36. Spolar, R. S., Livingstone, J. R., and Record, M. T., Jr. (1992) Use of liquid hydrocarbon and amide transfer data to estimate contributions to thermodynamic functions of protein folding from the removal of nonpolar and polar surface from water, *Biochemistry 31*, 3947−3955.
37. Sturtevant, J. M. (1977) Heat capacity and entropy changes in processes involving proteins, *Proc. Natl. Acad. Sci. U.S.A. 74*, 2236−2240.
38. den Blaauwen, T., van der Wolk, J. P., Van der Does, C., van Wely, K. H., and Driessen, A. J. M. (1999) Thermodynamics of nucleotide binding to NBS-I of the *Bacillus subtilis* preprotein translocase subunit SecA, *FEBS Lett. 458*, 145−150.
39. Kodama, T., and Woledge, R. C. (1976) Calorimetric studies of the interaction of myosin with ADP, *J. Biol. Chem. 251*, 7499−7503.
40. Urbatsch, I. L., Sankaran, B., Weber, J., and Senior, A. E. (1995) P-Glycoprotein is stably inhibited by vanadate-induced trapping of nucleotide at a single catalytic site, *J. Biol. Chem. 270*, 19383−19390.
41. Gaudet, R., and Wiley, D. C. (2001) Structure of the ABC ATPase domain of human TAP1, the transporter associated with antigen processing, *EMBO J. 20*, 4964−4972.
42. Karpowich, N., Martsinkevich, O., Millen, L., Yuan, Y. R., Dai, P. L., MacVey, K., Thomas, P. J., and Hunt, J. F. (2001) Crystal structures of the MJ1267 ATP binding cassette reveal an induced-fit effect at the ATPase active site of an ABC transporter, *Structure 9*, 571−586.
43. Yuan, Y. R., Blecker, S., Martsinkevich, O., Millen, L., Thomas, P. J., and Hunt, J. F. (2001) The crystal structure of the MJ0796 ATP-binding cassette. Implications for the structural consequences of ATP hydrolysis in the active site of an ABC transporter, *J. Biol. Chem. 276*, 32313−32321.

BI061230E